ISSN 1027-5495. Functional Materials, 30, No.3 (2023), p. 377-386.
doi:https://doi.org/10.15407/fm30.03.377

Preparation and properties of a lignocellulose nanocomposite material

Xingang Wang[1], *Zhongbo Liu*[2]

[1]Yulin Normal University, Guangxi, 537000 Yulin, China
[2]College of Railway Engineering, Jilin Railway Technology College, Jilin, 130000 Changchun, China

Received April 20, 2023

In this work, the Lignocellulose (LCS) matrix was intercalated into the nanoscale lamellar structure of montmorillonite (MTN) by the solution intercalation method, which completely destroyed the lamellar structure of MTN and made it uniformly dispersed in the LCS matrix in the form of nano-lamellar units, thus achieving an organic combination of LCS and MTN at the nanoscale and finally obtaining LCS/MTN nanocomposites. The results show that the XRD pattern of LCS/MTN has no obvious changes compared to LCS feedstock, indicating that oxalic acid hydrolysis did not destroy or alter the inherent crystalline structure of cellulose. LCS/MTN prepared at 50 wt% oxalic acid has a higher carboxyl content. This shows that the carboxyl content is not the main adverse factor affecting the thermal stability of LKS/MTH. The isotherm of dye adsorption by nanocomposites corresponds to the Langmuir isotherm, and all of them are less than 1, which corresponds to preferential adsorption. It can be used as an adsorbent to purify methylene blue dye in printing and dyeing wastewater.

Keywords: lignocellulose, nanocomposite, montmorillonite.

Отримання та властивості лігноцелюлозного нанокомпозитного матеріалу. *Xingang Wang, Zhongbo Liu*

У даній роботі матриця ЖКС була інтеркальована в нанорозмірну пластинчасту структуру монтморилоніту (МТН) методом інтеркалювання в розчині, що повністю зруйнувало пластинчасту структуру МТН і зробило його рівномірно диспергованим в матриці ЖКС у вигляді нано-пластинчастої одиниці, таким чином досягаючи органічного поєднання LCS та MTN на нанорівні та, нарешті, отримуючи нанокомпозити LCS/MTN. Результати показують, що рентгенограма LCS/MTN не має явних змін порівняно з сировиною LCS, що вказує на те, що гідроліз щавлевої кислоти не зруйнував та не змінив властиву целюлозі кристалічну структуру. LCS/MTN, приготований при концентрації щавлевої кислоти 50 мас.%, має вищий вміст карбоксилу. Це показує, що вміст карбоксилу не є основним несприятливим фактором, що впливає на термічну стабільність LCS/MTN. Ізотерма адсорбції барвника нанокомпозитами відповідає ізотермі Ленгмюра і всі вони менше 1, що відповідає переважної адсорбції. Його можна використовувати як адсорбент для очищення барвника метиленового синього у стічних водах друку та фарбування.

1. Introduction

In recent years, scientists all over the world are actively exploring the agricultural and forestry biomass resources to partially replace petrochemical resources, transforming production into energy and preparing chemical supplies and new materials [1–3]. Preparing new materials and new energy using biomass as raw material can also effectively reduce the greenhouse effect [4]. Wood fiber itself is a natural polymer material with the characteristics of low density, low price and good biodegradability.

In recent years, the rapid development of nanotechnology has promoted the progress of wood science and technology, and nanocomposite materials have become an inevitable trend of modern materials development. Tippktter, N. et al. obtained nano-cellulose whiskers by acid hydrolysis of cotton filter paper. However, the chemical method requires higher equipment and will cause pollution to the environment [5–6]. Borisova, A.S. et al. used quaternary ammonium salt cationic compound to organically modify bentonite. Through testing, it was found that the interlayer spacing of modified bentonite was increased compared with that of unmodified bentonite, which indicated that the modifier introduced into the interlayer of bentonite provides an intercalation effect [7]. Li, J. and others studied the adsorption performance of cellulose and its derivatives on urea, and the paper summarized the best synthesis conditions, adsorption conditions and adsorption mechanism of cellulose derivatives, which laid the foundation for medical treatment of uremia [8]. Santek, M. I. and others used polyvinyl alcohol (PVA) electrospun fiber modified by hemp cellulose nanowhiskers (LCNWs), and the preparation method of the material was simple and easy [9]. LCNWs is obtained by steam explosion, ball milling and ultrasonic to improve the mechanical properties of electrospun PVA nanofibers. Their research found that the tensile strength of PVA nanofibers reinforced by LCNWs increased by more than five times at the breaking point. Pang, B.I. and others prepared carboxylated cellulose nanocrystals (CNCs) from commercial microcrystalline cellulose by hydrolysis with mixed acid of citric acid and hydrochloric acid. The obtained CNCs samples have high crystallinity and good thermal stability [10]. Although it has some advantages to prepare CNCs with mixed acid of organic acid and inorganic acid, this method still does not solve the problem of acid recovery. Echeverria, C.A. and others used the sol-gel technology to prepare TiO_2/wood composites. The research showed that when the particle size of TiO_2 sol was about 2 nm, TiO_2 could enter the wood cell wall, and the thermal stability of the prepared TiO_2/wood composites was improved [11]. Han, J.K. et al. injected the precursor solution with silicon alkoxide as the main component into the wood sample pretreated by conventional pretreatment or coupling agent (GPTMS) by the sol-gel method, and under the reaction during heat treatment, silica nuclei formed in the wood cell wall, aggregated, and grew to form wood/silica nanocomposites. [12]. Kessler, M. Cai et al. successfully prepared 90 %(w/w/w) lignin nanofibers from lignin fibers by electrostatic spinning using aqueous dispersions of lignin, polyvinyl alcohol (PVA) and CNCs [13].

The contents of cellulose, hemicellulose and lignin are different in different LCS raw materials. LCS materials are abundant biomass resources on the earth, which have the advantages of renewability, biodegradability and biocompatibility. After derivative modification, LCS materials have been widely used in biomedicine, food, daily chemicals, aerospace, building materials and coatings, military industry and other fields [14–16]. LCS has great potential to solve food shortages, energy crisis, pollution and other problems facing humanity. Since LCS has rich hydroxyl groups in its molecular structure, it has a certain coordination or complexing effect on transition metals, and it is a good carrier material for transition metals or precious metals. In addition, LCS can be used as energy storage electrochemical and electrocatalytic materials after carbonization [17]. However, to date, there are not many commercialized LCS composites, which is limited mainly by the difficulties of processing LCS, the complex production process and the poor properties of the resulting materials. Therefore, further research is needed to develop new hemicellulose-based materials. In this paper, the LCS matrix was intercalated into the nano-scale lamellar structure of montmorillonite (MTN) by solution intercalation compound method, which completely destroyed the lamellar structure of MTN and made it uniformly dispersed in the LCS matrix in the form of nano-lamellar units, thus achieving an organic combination of LCS and MTN on the nano-scale. The prepared LCS/MTN compensated for the lack of uniform structure and characteristics of the raw materials and represented a new and effective nanocomposite adsorption material.

2. Application of LCS materials and theory of nanocomposites

2.1 Application of LCS materials

In addition to these three main components, LCS contains a small amount of protein, lipids, ash, pectin and some carbohydrates with low molecular weight. The interwoven structure of cellulose, hemicellulose and lignin ensures that the degradation of any component will be re-

stricted by other components [18]. They have different chemical compositions and properties, and the close cross-linking between them is also an important factor restricting the direct transformation of LCS into high value-added chemicals and new materials. In order to prepare nanocellulose with good properties, it is often necessary to pretreat LCS raw materials or the obtained nanocellulose. Pretreatment is beneficial to obtain individual CNFs and reduce energy consumption. Common pretreatment methods include sodium periodate oxidation, enzyme treatment and TEMPO oxidation [19–21].

In plants, lignin monomers are polymerized into lignin in various forms, and then cellulose is bonded together like an adhesive, giving plants a certain mechanical strength and the ability to resist external environmental invasion. One of the carbon-carbon polymerization methods makes the lignin structure very strong and difficult to be destroyed during decomposition. This not only affects the separation and extraction of lignin, but also seriously affects the output of lignin decomposition products. The structural schematic diagram of LCS is shown in Fig. 1.

According to its physical structure and composition, it can be divided into hard and soft categories. Broad-leaved forest is composed of three kinds of cells, namely, fiber cells, ducts and soft tissues. The honeycomb structure of fiber cells plays a supporting role, while the diameter of ducts is large, which facilitates the transport of water through the fiber cells. Bark contain a large number of tracheids and soft tissue cells that can provide mechanical support and transport water [22]. In addition, the structural differences of wood will also cause other differences in properties, the most obvious of which is density. The density of wood materials varies significantly with species, from the lightest balsa wood in the world with a density of 175 $kg \cdot m^{-3}$ to ebony with a density exceeding 1000 $kg \cdot m^{-3}$. Different densities lead to different porosity, which ultimately affects the properties of wood materials.

From the point of view of reaction kinetics, the condensation of lignin in the extraction process is always inevitable. Therefore, using cheap and easily available small molecules to condense with lignin is the only effective way to reduce the condensation of lignin itself. In the process of phenolic resin synthesis, if there is too much formaldehyde, the condensation will be terminated because the linking site is occupied by too much formaldehyde structure. Similarly, I found that formaldehyde and hydroxyl groups in lignin side chains can react quickly to form a stable six-membered ring structure, which prevents it from reacting with phenol structure [23].

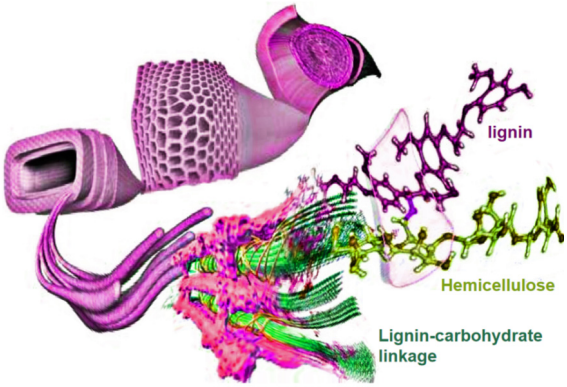

Fig. 1. Schematic diagram of LCS structure.

Solar steam power generation is widely used because of its renewable, environmentally friendly and other advantages. Using wood as solar steam power station can obtain good hydrophilicity, light weight, natural moisture transmission channel and good heat insulation performance [24–25]. The rather lengthy process of wood pretreatment, grinding, alcohol flame and cold water quenching [26] limits its large-scale production and application, and there is a need to find a simple and fast manufacturing method.

In nature, natural wood materials have good hydrophilicity and inherent microchannels. By simple in-situ treatment, they can not only retain their inherent microchannels, but also improve their hydrophilicity. In-situ treated LCS materials are applied to microfluidic analytical devices without additional channels, and rapid material transfer can be achieved by virtue of the capillary force generated by its inherent microchannels, and the anisotropic microstructure of wood materials will also cause anisotropic material transfer performance.

2.2.Nano-composite theory

Organic-inorganic nanocomposites are formed by high-precision compounding of organic and inorganic two-phase materials with different properties at nano or even molecular level. If the nano-composite technology of this kind of material is successfully introduced into the field of wood performance improvement, it is expected to

Table 1. Experimental materials

Name	Type	Factory
LCS		Beijing Ming ang Rui Xiang Technology Co., Ltd
MTN	CEC = 90 mol/100 g, 1100 mol/100 g, 110 mol/100 g	Zhejiang Fenghong Clay Chemical Co., Ltd.
muriatic acid	analytically pure	Shanghai Pilot Chemical Corporation
Anhydrous sodium acetate	analytically pure	Tianjin Fengchuan Chemical Reagent Co., Ltd
calcium carbonate	analytically pure	Sigma-Aldrich, St. Louis, MO, USA
sodium chloride	The purity is 99.5 %	Shanghai Aladdin Co., Ltd
sodium hydroxide	analytically pure	Tianjin Fengchuan Chemical Reagent Co., Ltd
Anhydrous oxalic acid	98 %	Sigma-Aldrich, St. Louis, MO, USA

provide the advantages of organic wood and inorganic materials simultaneously as a homogeneous nanocomposite with the synergistic effect, so that the modified wood can achieve high mechanical properties, superior durability, and even some functions or smart performance. Therefore, from the inevitable trend of deep cross-infiltration between nanotechnology and wood science, nano-composite of organic-inorganic materials and wood is undoubtedly one of the potential development directions of wood performance improvement.

Generally speaking, polymer/clay nanocomposites can be divided into three categories: 1) conventional compounding, clay maintains its original aggregation state, silicate lamellae of bentonite do not expand between layers, polymer macromolecules do not enter lamellae, and clay only plays the role of filler; 2) an intercalation nano-composite, in which the polymer enters bentonite particles, that is, between silicate lamellae, which increases the interlayer spacing, but the lamellae are still arranged neatly; 3) stripping composite: the polymer enters the clay lamellae, the lamellae are completely stripped, the laminated structure is destroyed, and the interlayer force disappears [27].

Physical adsorption and chemical adsorption often occur together, which is generally the result of the combination of the two kinds of adsorption in aqueous solution. However, due to the different types and properties of adsorbents and adsorbed substances, the adsorption process may be the leading role of one of them. By designing and calculating the adsorption data, the information of surface deformation of adsorption materials can be reflected, and the adsorption type can be determined by fitting and observing the coincidence degree of adsorption data.

3. Research method

3.1. Experimental materials

The main test materials in this paper are listed in Table 1.

3.2.Laboratory apparatus

The main experimental instruments and equipment in this paper are listed in Table 2.

3.3.Preparation of LCS nanocomposites

In this paper, the solution intercalation method was used to intercalate the LCS matrix into the nano-scale lamellar structure of MTN, which completely destroyed the lamellar structure of MTN and made it uniformly dispersed in the LCS matrix in the form of nano-lamellar units, thus the organic combination of LCS and MTN on the nano-scale was achieved. The prepared LCS/MTN compensated for the lack of uniform structure and characteristics of the raw materials, and represented a new and efficient nano-composite adsorption material. The preparation process of LCS/MTN nanocomposites in this paper is as follows:

1) 0.50 g MTN was weighed, dissolved in 15 mL distilled water, and stirred at room temperature for 30 min to form a uniform suspension.

2) 4.0 g MTN was added into 120 g distilled water, stirred by electric motor for 0.5 h, then slowly added into the NaOH suspension of LCS, heated and stirred continuously, and the experiment ended after a period of reaction.

3) The ratio of LCS to MTN was set at 3:1, 2:1, 1:2, 1:21and 1:3 respectively, and other conditions were set at 100 mmol/100 g CEC value of MTN, 20 %

Table 2

Name	Type	Factory
Electric mixer	D-60-2F	Hangzhou instrument electric machine factory
analytical balance	BS210S	Beijing Sai Dolis Tianping Co., Ltd.
centrifuge	SorvallRC-5BPlus	DuPont, Newtown, CT, USA
grinder	SJ-300	Zhejiang Dongfeng plastic machinery factory
circulating water vacuum pump	SHG-D(III)	Shanghai Shen Guang Instrument Co., Ltd
vacuum drying oven	DZF-6210	Shanghai Yiheng Scientific Instrument Co., ltd
PH tester	BPH-220	Hangzhou Liance Automation Technology Co., Ltd
XRD instrument	BrukerD8Discover	BrukerCo., Billerica, MA, USA
TG analyzer	Pyris1TGA	PerkinElmerInc., Waltham, MA, USA
Fourier transform infrared-near infrared spectrometer	Spectrum65	Perkin Elmer Enterprise Co., Ltd
High resolution projection electron microscope	JEM-2010	Japan Electronics Co., Ltd
Specific Surface Area and Pore Adsorption Instrument	ASAP2020	Micromeritics Corp
Electronic constant temperature water bath pot	TED	Tianjin taisite instrument Co., Ltd

NaOH mass concentration, 60°C reaction temperature and 6 h reaction time.

4) The concentration of NaOH solution was set at 0 %, 5 %, 15 %, 20 % and 25 % respectively, and other conditions were set at 100 mmol/100 g CEC value of MTN, 1:1 doping ratio of LCS and MTN, 60°C reaction temperature and 6 h reaction time.

5) According to the amount of methylene blue adsorption on LCS/MTN nanocomposites, the optimal preparation process of LCS/MTN nanocomposites was determined.

3.4.Characterization of properties of LCS nanocomposites

3.4.1. FTIR analysis

Fourier transform infrared spectroscopy (FTIR) was used to analyze LCS/MTN nanocomposites. A high-purity KBr tablet was added into a small number of samples, fully grinded and mixed evenly, pressed into transparent sheets with a tablet press; the spectra were recorded in the range to analyze the infrared absorption characteristics of the samples.

3.4.2. XRD analysis

X-ray diffraction (XRD) was used to study the LCS raw materials and LCS/MTN samples. The Cu–Kα X-ray source was used, the operating voltage and current were 50 kV and 1 mA respectively, the scanning range was 10–38°, and the scanning speed was 0.02° s^{-1}. The crystallization index *CrI* was calculated according to the empirical method:

$$CrI = \frac{I_{200} - I_{at}}{I_{200}} \cdot 100\%, \quad (1)$$

where I_{200} is the maximum peak intensity of the (200) diffraction reflection, and I_{at} is the minimum diffraction intensity between reflections (110) and (200).

3.4.3. TG analysis

Thermogravimetric (TG) testing of LCS raw materials and prepared LCS/MTN samples was carried out by a TG analyzer. The heating rate is 10°C·min^{-1}, the temperature test range is 50–600°C, and the flow rate is 20 mL·min^{-1} under nitrogen protection. Before the test, all the samples were dried at 50°C for 4 h to remove water.

3.4.4. Adsorption performance test

0.1000 g LCS was accurately weighed and put it into a 100 mL conical flask; 25 mL dye solution with known concentration was added, and the mixture was placed

in a constant temperature oscillator (120 r/min) to achieve adsorption equilibrium under certain conditions; it was then centrifuged, the concentration of supernatant was measured by spectrophotometry, and the adsorption amount Q_1 (mg/g) was calculated as follows:

$$Q_1 = \frac{(C_0 - C_t) \cdot V}{m}, \quad (2)$$

where Q_1 is the adsorption amount (mg/g), C_0 is the initial concentration of the solution (mg/L), C_t is the concentration of residual ions in the solution after adsorption (mg/L), m is the dosage of adsorbent (g), and V is the volume of ion solution (L).

3.4.5. Testing mechanical properties

A domestic CSS-44100 universal material testing machine was used to apply axial static tensile load to the sample until the maximum tensile stress that the sample experiences upon failure, called the ultimate strength of the material, is reached. The tensile strength value is calculated according to the following formula:

$$\sigma_t = \frac{F}{bd(MPa)}, \quad (3)$$

where F is the maximum tensile load (N) of the sample; b is the sample width (m); d is the sample thickness (m).

The static bending strength and flexural elastic modulus of composites were measured by using domestic CSS-44100 universal material testing machine. They are calculated as follows:

$$\sigma_b = \frac{3 \cdot P_{\max} \cdot l}{2 \cdot b \cdot h^2} \quad (4)$$

where σ_b is the static bending strength of the specimen, MPa; P_{max} is the maximum load when the specimen is damaged, N; l is the distance between two supports, mm; b is the sample width (m); h is the sample thickness (m).

$$\frac{l^3}{4 \cdot b \cdot h^3} \cdot \frac{\Delta f}{\Delta s}, \quad (5)$$

where E_b is the flexural elastic modulus of the specimen, MPa; l is the distance between two supports, mm; b is the sample width (m); h is the sample thickness (m); Δf is the increase of the internal force of the straight line segment in the load-deformation diagram, N; Δs deformation of specimen in force $f_2 \sim f_1$ interval, mm.

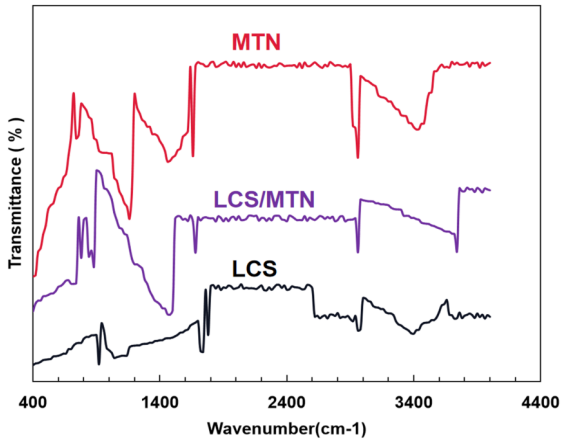

Fig. 2. Infrared spectra of LCS, MTN and LCS/MTN nanocomposites.

4. Results and discussion

4.1.FTIR Characterization of LCS/MTN

Infrared spectrum can be divided into a functional group region (wave number is 4000–1300 cm^{-1}) and a fingerprint region (wave number is 1300–650 cm^{-1}). Each infrared absorption peak in the functional group region corresponds to a certain functional group, which is the main basis for infrared spectrum analysis. Fig. 2 shows the infrared spectra of LCS, MTN and LCS/MTN nano-composite adsorption materials respectively.

It can be seen that after the intercalation compound reaction between MTN and LCS, the stretching vibration peak of -OH at 3459 widens and drifts to the high wavenumber direction at 3498 cm^{-1}. The O–H absorption peak of H_2O in MTN at 1673 cm^{-1} shifts to a high wavenumber of 1690 cm^{-1}. At the same time, the absorption peak of Si–O bond stretching vibration of MTN at 1055 cm^{-1} shifts to the low wavenumber 1095 cm^{-1}. In LCS/MTN nanocomposites, a new absorption peak appeared at 1890 cm^{-1}, which belongs to the stretching vibration absorption peak of C=O [10].

These changes indicate that the -OH, Si–?O bonds in MTN and the C–O and C–O–O bonds in LCS may undergo ion exchange or coordination complexation through cations between MTN sheets in the alkaline solution. The long molecular chains of the LCS matrix have destroyed the nano-scale lamellar structure of MTN, and intercalated into the interlayer domain of MTN, forming an

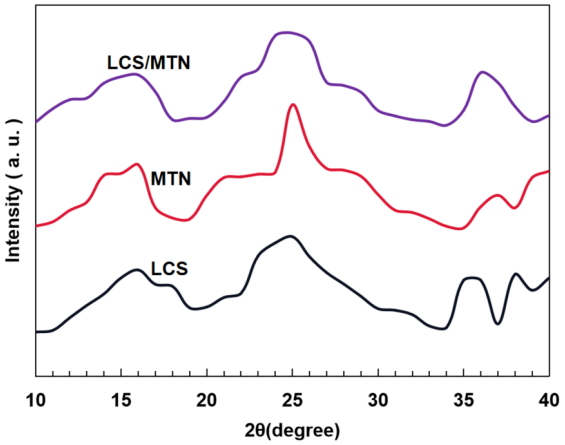

Fig. 3. XRD spectra of LCS raw materials and corresponding LCS/MTN.

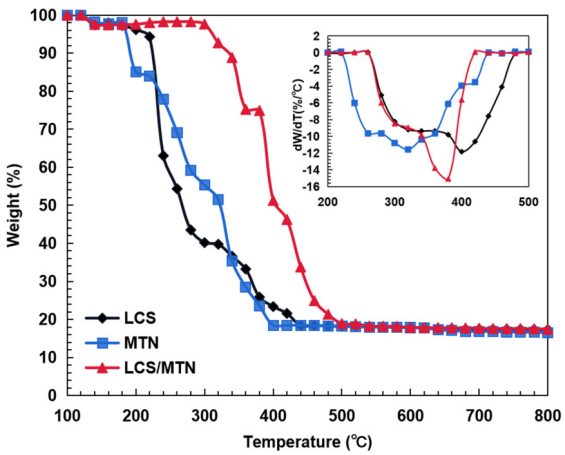

Fig. 4. TG of LCS raw materials and corresponding LCS/MTN.

intercalated-exfoliated LCS/MTN nano-composite adsorption material with many new active functional groups such as -OH, -C=O, C–O–C, –COOH, etc., and the chemical composition and structure have changed greatly.

4.2.Crystallinity of LCS/MTN

Figure 3 shows the XRD patterns of LCS raw materials and corresponding LCS/MTN.

As can be seen from the figure, LCS and MTN and the corresponding LCS/MTN have three characteristic peaks at about 16.8°, 22.5° and 34.6°, which respectively correspond to the (110), (200) and (004) reflection planes of the typical cellulose I-type structure [25]. Compared with LCS raw materials, the XRD pattern of LCS/MTN showed no obvious changes, indicating that oxalic acid hydrolysis did not destroy or change the inherent crystal structure of cellulose.

CrI values are calculated from XRD and FTIR spectra respectively and listed in Table 3.

It can be seen that the *CrI* values of LCS and MTN raw materials calculated by XRD patterns are 76.932 and 77.266 %, respectively. Compared with the *CrI* values of LCS and MTN, the *CrI* values of LCS/MTN prepared from them did not change significantly.

On the other hand, the *CrI* data obtained by FTIR test show that the crystallinity of LCS/MTN obtained from LCS and MTN is slightly reduced, which may be related to the higher crystallinity of cellulose II structure of LCS/MTN [24].

4.3.Thermal stability of LCS/MTN

TG curves of LCS raw materials and corresponding LCS/MTN are shown in Fig. 4.

The thermal decomposition of cellulose includes depolymerization, dehydration and decomposition of glycosyl units and the subsequent formation of carbonized residues [16]. The high surface area of LCS/MTN increases their contact area with heat, so it may also play an important role in reducing their thermal stability [19].

LCS/MTN prepared at 50 wt% oxalic acid concentration has higher carboxyl content, but their initial decomposition temperature is higher than that prepared at the 30 wt% concentration of oxalic acid. These results show that the carboxyl content is not the main unfavorable factor affecting the thermal stability of LCS/MTN.

4.4. Analysis of dye adsorption isotherm of LCS/MTN nanocomposites

Table 3. Crystallinity and thermal stability data of LCS raw materials and corresponding LCS/MTN

Sample	*CrI*, %		5 % mass loss temperature	Initial decomposition temperature
	XRD	FTIR		
LCS	76.932	65.42	270	273.3
MTN	77.266	71.131	355.3	253.6
LCS/MTN	75.62	58.209	309.4	315.4

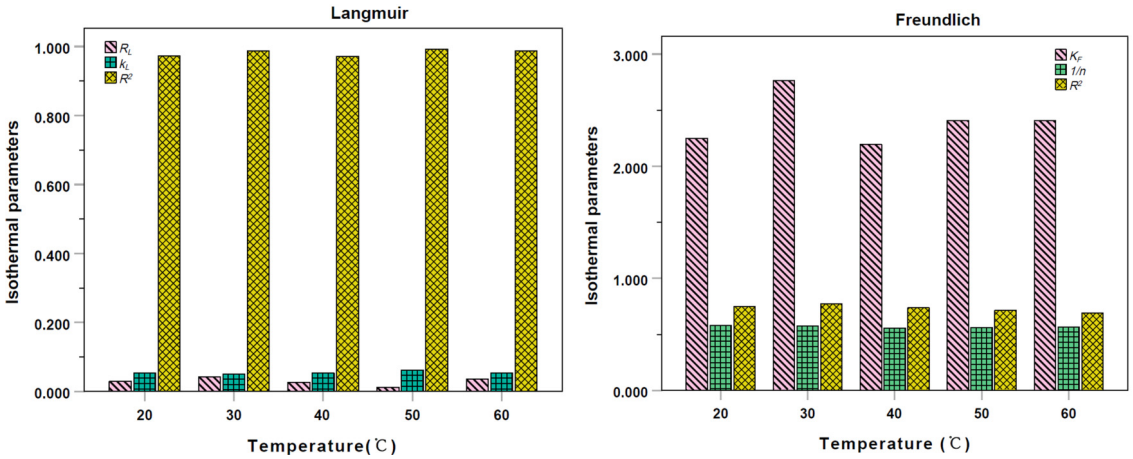

Fig. 5. Isothermal parameters of methylene blue adsorption by nanocomposites at different adsorption temperatures.

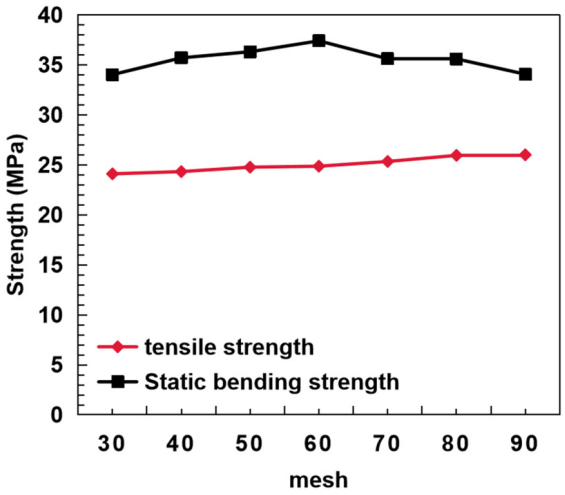

Fig. 6. Effect of particle size on mechanical properties of composites.

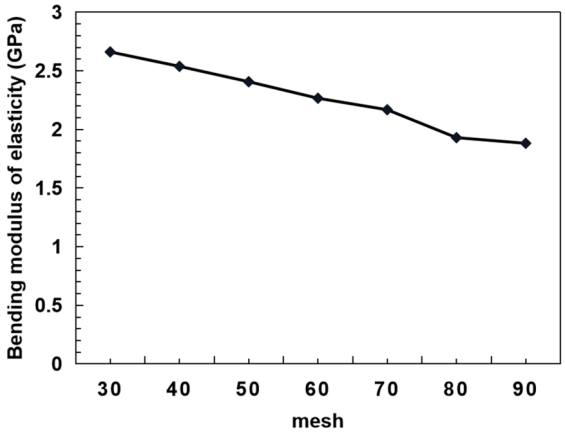

Fig.7. Effect of particle size on flexural elastic modulus of composites.

Adsorption conditions of methylene blue: concentration of 1200, 1300, 1400, 1500 and 1600 mg/L, pH of 6, and adsorption time of 300 min. The results of adsorption isotherm equation parameters of methylene blue adsorbed by nanocomposites at different adsorption temperatures are shown in Fig. 5.

From the correlation coefficient R^2 of Langmuir and Freundlich isotherms, it can be seen that the correlation coefficient of the Langmuir isotherm is better than the Freundlich isotherm when it reaches more than 0.98; this shows that the adsorption isotherm of dyes by nanocomposites conforms to the Langmuir isotherm and represents single-layer adsorption.

The values of R_L are 0.029, 0.042, 0.026, 0.012 and 0.036 at temperatures of 20, 30, 40, 50 and 60°C, respectively. All less than 1 correspond to preferential adsorption. The results show that nanocomposites can be used as an adsorbent to treat methylene blue dye in printing and dyeing wastewater.

4.5. Effect of different particle sizes on mechanical properties of LCS/MTN nanocomposites

Fig. 6 shows a graph of tensile strength and flexural strength of LCS/MTN nanocomposites with different particle sizes at a content of 30 %. When 60-mesh LCS filled with MTN, the static bending strength of the composites reached 37.408 MPa, and the tensile strength of 90-mesh LCS/MTN nanocomposites reached a maximum of 26.01 MPa.

Fig. 7 shows a graph of bending elastic modulus of LCS/MTN nanocomposites with different particle sizes. The bending elastic modulus of 30 mesh LCS/MTN nanocomposites is the largest, and the elastic modulus decreases with an increase in the particle size.

LCS particles of different sizes are subject to different forces during the crushing process, so LCS particles of different sizes have different surface roughness and aspect ratio [10]. In order to make LCS particles well infiltrated by MTN, the particle size of LCS must be selected in a suitable range.

According to the principle of fiber reinforcement, the smaller the particle size of filler, the more uniform the dispersion and the better the mechanical properties of composite materials. However, the smaller the particle size, the more difficult it is to achieve uniform dispersion, requiring more additives and better processing equipment, and the finer the particles, the higher the processing cost. LCS with large particle size and high roughness is easy to form void defects at the interface.

5. Conclusions

The LCS/MTN nanocomposites prepared in this paper make up for the lack of structural properties of a single raw material, and are a new and efficient nanocomposite adsorption material. After a large number of comprehensive experiments, the following conclusions are obtained: the long macromolecular chain of the LCS matrix destroys the nano-scale lamellar structure of MTN, and intercalation enters the interlayer domain of MTN, forming an intercalated-exfoliated LCS/MTN nano-composite adsorption material with many new active functional groups and great changes in chemical composition and structure. Compared with LCS raw materials, the XRD pattern of LCS/MTN shows no obvious changes, indicating that oxalic acid hydrolysis has not destroyed or changed the inherent crystal structure of cellulose. LCS/MTN prepared at 50 wt% oxalic acid concentration has a higher carboxyl content. This shows that the carboxyl content is not the main unfavorable factor affecting the thermal stability of LCS/MTN. The isotherm of dye adsorption by nanocomposites corresponds to the Langmuir isotherm, and the values are 0.029, 0.042, 0.026, 0.012 and 0.036 at temperatures of 20, 30, 40, 50 and 60°C, respectively. All the values less than 1 correspond to preferential adsorption. The results show that nanocomposites can be used as an adsorbent to treat methylene blue dye in printing and dyeing wastewater. Different particle sizes of LCS are subject to different forces in the crushing process, so different particle sizes of LCS have different surface roughness and aspect ratio. In order to make LCS particles well infiltrated by MTN, the particle size of LCS must be selected in a suitable range.

In order to further improve the application scope of research and application, rapid and accurate adsorption materials, the current nano-composite materials should be used to adsorb other heavy metal ions, industrial oil pollution and dye pollutants in the future to study the scope and effect of this material. Nano-LCS is applied to the polymerization of other materials to change the physical, chemical and mechanical properties of raw materials.

Acknowledgements. This work is supported by Scientific Research Project: Quantitative study on forest ecological compensation benefits (Grant No. G2022sk23).

References

1. Z.Wang, X.Shen, Y.Yan et al., *Applied Surface Science*, **450**, 30 (2018).
2. X.Xu, J.Gan, Y.Huang et al., *Functional Materials Letters*, **15**, 1 (2022).
3. K.Li, Y.Wang, X.Li et al., *Chemosphere*, **302**, 9 (2022).
4. M.L.Testa, M.L.Tummino, *Catalysts*, **11**, 1 (2021).
5. N.Tippktter, J.Roth, *Chemie Ingenieur Technik*, **92**, 11 (2020).
6. L.Peng, X.Huangfu, Y.Liu et al., *Renewable Energy*, **193**, 6 (2022).
7. A.S.Borisova, E.V.Eneyskaya, S.Jana et al., *Biotechnology for Biofuels*, **11**, 1 (2018).
8. J.Li, D.J.W.Lawton, G.G.Sacripante et al., *Industrial Engineering Chemistry Research*, **60**, 38 (2021).
9. M.I.Santek, M.Grubisic, M.G.Perecinec et al., *Process Biochemistry*, **109**, 10 (2021).
10. B.Pang, Z.Sun, L.Wang et al., *Chemical Engineering Journal*, **95**, 1 (2021).
11. C.A.Echeverria, F.Pahlevani, V.Sahajwalla, *J. Cleaner Production*, **258**, 54 (2020).
12. J.K.Han, A.Madhusudhan, R.Bandi et al., *Bioresources*, **15**, 2 (2020).
13. M.Kessler, R.Ahorsu, F.M.Medina, *Chemie Ingenieur Technik*, **92**, 9 (2020).
14. K.Kepa, C.M.Chaleat, N.Amiralian et al., *Cellulose*, **26**, 11 (2020).
15. Y.Ding, B.Shan, X.Cao et al., *J.Cleaner Production*, **288**, 3 (2020).
16. Y.Zhou, J.Yang, C.Luo et al., *Bioresources*, **14**, 1 (2019).
17. A.H.Aly, H.A.Elsayed, C.Malek, *Optica Applicata*, **48**, 1 (2018).
18. J.Li, L.Xu, J.He et al., *New J.Chemistry*, **10**, 1039 (2018).
19. C.Y.Shao, M.Wang, H.L.Chang et al., *Chem. Mater.*, **30**, 9 (2018).

20. S.A.Malyshev, O.A.Shlyakhtin, G.N.Mazo et al., *Functional Materials Letters*, **10**, 06 (2018).
21. L.Fotouhi, P.S.Dorraji, Y.S.S.Keshmiri et al., *Electrochemical Society*, **165**, 5 (2018).
22. B.D.Chen, T.Zhou, Z.L.Wang et al., *Nano Research*, **11**, 6 (2018).
23. L.Yamei, H.Caili, J.Tifeng et al., *Nanomaterials*, **8**, 1 (2018).
24. N.Shandilya, O.L.Bihan, M.Morgeneyer, *J. Nanomaterials*, **2014**, 1 (2018). .
25. B.Jiang, L.Li, Z.Bian et al., *Intern. J. Hydrogen Energy*, **43**, 29 (2018).
26. Z.Y.Ding, F.F.Wen, J.L.Wang et al., *Green Chem.*, **20**, 6 (2018).
27. W.Cui, T.Tobimatsu, Saucet et al., *New Phytol.*, **218**, 2 (2018).